

## Supplementary Text

### 1. Contributions from carbon and nitrogen atoms and cage components.

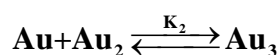
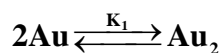
Since a gold atom has much more electrons (79 electrons) than a carbon (6 electrons) or a nitrogen (7 electrons) atom, the scattering intensity from gold atoms is expected to be much stronger than the scattering intensity from carbon or nitrogen atoms. We calculated the scattering intensities from carbon and nitrogen atoms using the same methods described in Method section and compared them with the scattering intensity from gold atoms in Extended Data Figure 6a. As expected based on the number of electrons in each atom, the scattering intensities from carbon and nitrogen atoms are negligibly small compared with the scattering from gold atoms. As a result, the total scattering intensity combining the contributions of all the atoms in  $[\text{Au}(\text{CN})_2^-]_3$  is almost identical to the scattering from gold atoms only.

We made a similar comparison between solute and cage contributions as shown in Extended Data Figure 6b. Scattering from the cage term is also expected to be negligible because (1) the scattering from gold atoms is much stronger than the scattering from oxygen atoms in solvent molecules and (2) the cage term mainly arises from oxygen-carbon and oxygen-nitrogen atomic pairs since gold atoms are surrounded by  $\text{CN}^-$  ligands. The cage term was calculated from the pair distribution functions between solute and solvent molecules obtained from molecular dynamics simulations. As expected, the cage term is negligibly small compared with the solute-only term and the total scattering intensity combining both solute-only and cage terms is almost the same as the solute-only term. Thus, we can conclude that the experimental scattering signal after subtraction of solvent heating contribution is dominated by the contribution of Au-Au pairs only.

### 2. Determination of dimer contribution

In the previous TA study,<sup>5</sup>  $[\text{Au}(\text{CN})_2^-]_3$  trimer was selectively excited by laser pulses at 310 nm wavelength. In contrast, in this work, we used the laser excitation at 267 nm in order to achieve a higher quantum yield of the photoinduced reaction and thus higher signal-to-noise ratio. However, if the signal contribution from the  $[\text{Au}(\text{CN})_2^-]_2$  dimer is significant, it can complicate the analysis of the transient signal for the photoreaction of  $[\text{Au}(\text{CN})_2^-]_3$  trimer. In order to account for this issue, we calculated the expected contribution of the dimer to the time-resolved X-ray scattering signal. Since the high concentration (0.3 M) of our sample solution leads to very high absorbance ( $\gg 1$ ), we cannot use the method used for

determining the contribution of gold dimer,  $[\text{Au}(\text{CN})_2^-]_2$ , to the (pump-probe) transient signals in the previous TA study.<sup>5</sup> Instead, we devised a following method to estimate the contribution of dimer excitation quantitatively. The equilibriums among monomer, dimer and trimer can be written as follows,



where Au represents a monomer unit of the gold complex,  $[\text{Au}(\text{CN})_2^-]$ , and  $K_1$  and  $K_2$  are the equilibrium constants for the monomer–dimer and dimer–trimer equilibriums, respectively. If we assume that the contributions from higher oligomers are negligible, we can obtain the following equations for the concentrations of the three species.

$$[\text{Au}] + 2[\text{Au}_2] + 3[\text{Au}_3] = c \quad (1)$$

$$K_1 = \frac{[\text{Au}_2]}{[\text{Au}]^2} \quad (2)$$

$$K_2 = \frac{[\text{Au}_3]}{[\text{Au}][\text{Au}_2]} \quad (3)$$

where  $c$  is the initial concentration of monomers. By substituting Eqs. (1) and (2) into Eq. (3), we obtain

$$3K_1K_2[\text{Au}]^3 + 2K_1[\text{Au}]^2 + [\text{Au}] - c = 0 \quad (4)$$

The concentration of monomers,  $[\text{Au}]$ , can be obtained by solving Eq. (4) and thus can be expressed in terms of  $K_1$ ,  $K_2$  and  $c$ . Since the value of  $K_1$  was reported to be  $17.9 \text{ M}^{-1}$  and  $c$  is an experimental variable (for example,  $c = 0.3 \text{ M}$  in our experiment and  $c$  varies from  $0.00018 \text{ M}$  to  $0.28 \text{ M}$  in the previous TA study),  $K_2$  is the only parameter that needs to be determined. Once  $[\text{Au}]$  is determined,  $[\text{Au}_2]$  and  $[\text{Au}_3]$  can be readily calculated by the following two relations derived from Eq. (2) and Eq. (1), respectively.

$$[\text{Au}_2] = K_1[\text{Au}]^2 \quad (5)$$

$$[\text{Au}_3] = \frac{1}{3}(c - [\text{Au}] - 2K_1[\text{Au}]^2) \quad (6)$$

From these equations, we calculated the concentrations of the three species as a function of  $c$  as shown in Extended Data Figure 7a, where  $c$  was varied from zero to  $0.4 \text{ M}$  and  $K_2$  was assumed to be  $10 \text{ M}^{-2}$ .

Meanwhile, the relationship between the concentrations and the absorption (at a certain wavelength) of the three species can be written as follows:

$$\varepsilon_{\text{Au}} \mathbf{d}[\text{Au}]_c + \varepsilon_{\text{Au}_2} \mathbf{d}[\text{Au}_2]_c + \varepsilon_{\text{Au}_3} \mathbf{d}[\text{Au}_3]_c = \mathbf{A}_c \quad (7)$$

Here  $\varepsilon_{\text{Au}}$ ,  $\varepsilon_{\text{Au}_2}$ , and  $\varepsilon_{\text{Au}_3}$  are the extinction coefficients of the monomer, dimer and trimer, respectively,  $d$  is the path length of the sample solution, and  $A_c$  is the absorbance at a given  $c$ . Since  $\varepsilon_{\text{Au}}$  at 267 nm is negligibly small and the path length used in the previous TA study was 0.05 cm, Eq. (7) can be simplified to:

$$\varepsilon_{\text{Au}_2} [\text{Au}_2]_c + \varepsilon_{\text{Au}_3} [\text{Au}_3]_c = 20\mathbf{A}_c \quad (8)$$

From Fig. S1 of the previous TA study,<sup>5</sup> we can find at least four points ( $A_1$ ,  $A_2$ ,  $A_3$ , and  $A_4$ ) that can be used as inputs for Eq. (8) at the wavelength of 267 nm as shown in Extended Data Figure 7b. When we input the  $c$  and  $A_c$  values at  $A_1$ ,  $A_2$ ,  $A_3$ , and  $A_4$  into Eq. (8), we obtain the following four equations.

$$\varepsilon_{\text{Au}_2} [\text{Au}_2]_{c=0.013\text{M}} + \varepsilon_{\text{Au}_3} [\text{Au}_3]_{c=0.013\text{M}} = 0.5 \quad (9)$$

$$\varepsilon_{\text{Au}_2} [\text{Au}_2]_{c=0.027\text{M}} + \varepsilon_{\text{Au}_3} [\text{Au}_3]_{c=0.027\text{M}} = 2 \quad (10)$$

$$\varepsilon_{\text{Au}_2} [\text{Au}_2]_{c=0.054\text{M}} + \varepsilon_{\text{Au}_3} [\text{Au}_3]_{c=0.054\text{M}} = 8 \quad (11)$$

$$\varepsilon_{\text{Au}_2} [\text{Au}_2]_{c=0.075\text{M}} + \varepsilon_{\text{Au}_3} [\text{Au}_3]_{c=0.075\text{M}} = 16 \quad (12)$$

As we mentioned earlier,  $[\text{Au}]$ ,  $[\text{Au}_2]$ , and  $[\text{Au}_3]$  can be calculated as a function of  $c$  when the value of  $K_2$  is given. Therefore, the unknown parameters in these four equations are  $K_2$ ,  $\varepsilon_{\text{Au}_2}$ , and  $\varepsilon_{\text{Au}_3}$ . Since we have three unknown parameters and four equations, we can readily determine the values of  $K_2$ ,  $\varepsilon_{\text{Au}_2}$ , and  $\varepsilon_{\text{Au}_3}$  at 267 nm. We applied a least-square-fitting method by using MINUIT code to optimize the values of the three unknown parameters. The optimized values are  $K_2 = 8.0 \text{ M}^{-2}$ ,  $\varepsilon_{\text{Au}_2} = 1.2 \times 10^2 \text{ cm}^{-1}\text{M}^{-1}$ ,  $\varepsilon_{\text{Au}_3} = 3.2 \times 10^3 \text{ cm}^{-1}\text{M}^{-1}$ . Based on these values, we calculated theoretical difference scattering curves for the trimer and the dimer as shown in Extended Data Figure 7c while estimating the relative intensities of the two curves realistically based on the excitation probabilities and the equilibrium of the two species. Using these scattering curves of the dimer and the trimer, we can determine the contribution of the dimer species to our scattering signal by using the following equation.

$$\% \text{ of dimer signal} = \frac{\sum_q q |\Delta S_{\text{Au}_2}(q)|}{\sum_q q |\Delta S_{\text{Au}_2}(q)| + \sum_q q |\Delta S_{\text{Au}_3}(q)|} \times 100 \quad (13)$$

The dimer contribution was determined to be only 2.9 % and thus should be negligible.

### 3. Excitation wavelength dependence of reaction mechanism

In the previous section, we showed that the dimer contribution to our TRXSS signal should be negligible. In order to confirm this finding, we also measured TRXSS data with 310 nm excitation. The results for the 267 nm and 310 nm excitation conditions are compared in Extended Data Figure 8. Right singular vectors obtained from the SVD analysis for the two excitation wavelengths were fitted by exponentials as shown in Extended Data Figure 8a. Only one kinetic component was identified for both cases and the extracted time constants are almost identical (1.9 ps for 310 nm excitation and 1.6 ps for 267 nm excitation) to each other. Also, the difference scattering curves at 100 ps time delay measured with 310 nm (black) and 267 nm (red) excitation wavelengths are compared in Extended Data Figure 8b and it can be seen that the two curves are identical to each other within the experimental error. The same kinetics and the same shape of the difference scattering curves for the two excitation wavelengths indicate that the contribution of the dimer is negligible.

### 4. Comparison with the TA study

The previous TA study<sup>5</sup> showed the changes of transient absorption on multiple time scales. Based on the measured time constants and the theoretical UV-vis spectra, the mechanism described in Extended Data Figure 9 was suggested for the Au-Au bond formation in  $[\text{Au}(\text{CN})_2^-]_3$ . The time scales of the transitions found in the TA study match well with the results of this work, and our proposed reaction mechanism is consistent with the one proposed in the TA study as shown in Extended Data Figure 9, except for the structural assignments on the early kinetics. In particular, from our TRXSS measurement, the bent-to-linear transition was found to occur within a few hundred femtoseconds rather than on the time scale of 2 ps. Considering that TRXSS is only sensitive to the processes accompanying structural change, the intersystem crossing processes on ~500 fs and 13 ns time scales, which were not observed in the TRXSS measurement, are likely to involve no structural change..

## 5. Structural fitting analysis with Debye-Waller factor

In the main text, the nonequality of  $R_{12}$  and  $R_{23}$  in the  $S_0$  state is interpreted to result from broadening of the radial distribution function induced by relatively free movements of weakly bound Au atoms. To validate this interpretation, we performed additional structural fitting analysis by considering a constraint of the symmetric structure ( $R_{12} = R_{23}$ ) and a Debye-Waller factor for the  $S_0$  state. When including the Debye-Waller factor,  $\exp(-\sigma^2 q^2/2)$ , Eq. (7) in the Methods section is modified as follows.

$$r^2 S_{theory}(r) = \sum_{i=1}^n \frac{r}{2\pi^2} \int_0^\infty q F_{Au}^2(q) \frac{\sin qR_i}{qR_i} \sin(qr) e^{-\frac{\sigma^2 q^2}{2}} e^{-q^2 \alpha} dq \quad (14)$$

where  $\sigma^2$  is the mean-squared displacement. The theoretical RDFs were calculated by Eq. (14) and used for the structural fitting analysis.

In the fitting results summarized in Extended Data Figure 10, it can be seen that the theoretical and the experimental species-associated RDFs are in good agreement with each other. The obtained mean-squared displacement ( $\sigma^2$ ) is  $0.49 \text{ \AA}^2$ , which is much larger than the value for Au crystals ( $0.02 \text{ \AA}^2$ ), indicating the possible involvement of large-amplitude vibrations. Notably, the structural parameters of  $S_1$ ,  $T_1$ , and tetramer obtained from this structural fitting analysis are similar to the values obtained from the analysis without any structural constraint shown in Figure 2d. Thus, the seemingly asymmetric structure of the  $S_0$  state is likely to arise from broadening of the RDF of the  $S_0$  state induced by large-amplitude vibrations of weakly bound Au atoms.